ISSN 0025-6544, Mechanics of Solids, 2026, Vol. 61:168. © Pleiades Publishing, Ltd., 2026.

Investigation of Free Vibrations of a Hollow Cylinder under Different Boundary Conditions Using the Method of Potentials

Betül Uysal[a], Hüseyin Yıldız[a], Erol Uzal[a], Birkan Durak[a], Ali Serdar Gültek[a], Mana Sezdi[a], Serdar Yılmaz[a,*], and Sule Kapkin[a]

[a] *Istanbul University-Cerrahpasa, Istanbul, 34320 Turkiye*

**e-mail: serdar.yilmaz@iuc.edu.tr*

Received October 30, 2025; revised April 27, 2026; accepted April 28, 2026

Abstract—Cylindrical structural elements are widely used in aerospace and civil engineering applications due to their high structural efficiency. In this study, the free vibration behavior of thick-walled, homogeneous, and isotropic hollow cylinders is analytically investigated using the displacement potentials of the Navier–Lamé equations. Four different boundary-condition models free–free, fixed–free, fixed–fixed and free–fixed are systematically compared. The variation of dimensionless frequencies with respect to the wave number is calculated, and the frequency curves, radial displacement distributions, and variations of stress components along the cylinder thickness are presented graphically. The results show that boundary conditions have a significant influence on the dynamic behavior of the cylinder. While the natural frequencies take higher values in constrained models, lower frequencies are observed in models with free boundary conditions. Furthermore, as the wave number increases, the frequency curves corresponding to different boundary conditions converge. It is also shown that the displacement amplitudes and stress distributions depend strongly on the boundary conditions. The obtained analytical results provide a reliable reference for validating numerical models of hollow cylindrical structures and contribute to the analytical investigation of cylindrical pipes and multilayer pipe systems with similar geometries.

Keywords: cylinder vibration, potentials solution, numerical solution, Navier-Lamé equations, Shell

DOI: 10.1134/S002565442560641X

1. INTRODUCTION

Cylindrical shells are encountered in various engineering disciplines, including mechanical, civil and chemical engineering. These are utilized in many applications, including space frame systems in architecture and civil engineering, power transmission components in mechanical engineering, petro-chemical applications, liquid fuel tanks and biomedical applications such as prosthetic design. Additionally, cylindrical shells are found in sugar and cement silos, liquid balancing tanks, missiles, rockets and spacecraft. Due to their lightweight nature and structural efficiency, these components are utilized in a variety of engineering fields, such as high-pressure vessels, pipeline structures, heat exchangers and aircraft fuselages [1].

Researchers have examined the axial, symmetric and bending vibrations of thick and thin-walled cylinders made of different materials using various analytical and numerical methods. In recent developments, sandwich cylindrical shells consisting of integrated angled ribs between laminate surface layers have been employed in various applications, including spacecraft, automobiles and construction, to obtain high stiffness-to-mass ratios. Incorporating ultra-low-density cores into these structures offers additional advantages, including weight loss and improved energy dissipation [2]. Adding silica nanoparticles to composite cylindrical shells improves their mechanical properties. Nanomaterial-reinforced composite shell structures exhibit significant dynamic changes, with the natural frequency of shell structures increasing with a higher volume ratio of nanomaterials [3]. Lightness is a crucial design criterion in the aerospace industry. Consequently, carbon fiber-reinforced composite cylindrical shells, including stiffened and sandwich shells, are frequently used in the manufacture of aerospace products such as satellites and space rockets, due to their lightweight nature [4].

Comprehensive research to establish the mathematical foundation of determining free vibration of longitudinal objects was primarily conducted by Gazis [5] focusing on the propagation of waves. His studies

led him to publish a reference textbook along with [6]. Some researchers studied and explored hollow elastic rods [7] while others studied solid rods [8–10]. Stiffness of a rod is a major topic in vibration analysis. Eisenberger [11] presented a method to determine the natural frequencies at which the stiffness of a rod becomes zero in his work. Similarly, Abrate [12] evaluated simplified formulas for the analytical solution of free rods and rods connected at one end. Variable cross sections have been an appealing subject for many researchers. Kumar and Sujith [13] examined the dependence of the solution, considering whether the end of the rod is connected or not. Raj and Sujith [14] evaluated the natural frequencies of free-end and end-bonded variable cross-section rods. Gladwell and Vijay [15] presented the lowest frequencies as a functional relationship between the length, radius and thickness of the material under investigation. The study of the movements of cylinders subjected to specific loadings and vibrations remains a relevant topic. Although cylindrical shells are frequently used in various engineering branches, analyzing their dynamic characteristics is quite complex. This complexity stems from the coupled differential equations that govern shell motion and from the sensitivity of the response to boundary conditions [16]. Because this sensitivity becomes even more pronounced for thick-walled configurations, there has been a clear shift from simplified shell theories toward three-dimensional (3D) elasticity-based formulations. Asgari [17] showed that such 3D frameworks are essential to accurately predict the natural modes of hollow cylinders by capturing complex displacement fields and vibrational behaviors that lower-dimensional assumptions can overlook. In practical engineering systems, cylindrical shells rarely exist in isolation; they are typically joined to other components through a wide variety of connection details. As a result, boundary conditions are often non-classical, making their realistic representation a central research focus. A common and effective way to model these non-classical constraints is to attach artificial springs with suitably chosen stiffness values at the shell ends, enabling the simulation of arbitrary boundary conditions [18].

Paimushin and Shishkin [19] studied forced bending vibrations of a flat rod with two cantilevers and a finite-length fixed region, emphasizing that the kinematic coupling at the free–fixed transition can strongly influence the response. Using an exact analytical solution based on the Hamilton–Ostrogradsky principle, they showed that including transverse compression in the fixed region can markedly increase resonance amplitudes in metal rods, while the effect is more limited in composite rods. Leizerovich and Taranukha [20] analyzed nonlinear free bending vibrations of a thin-walled circular cylindrical shell with hinged ends and showed that large-amplitude bending is inherently coupled with radial motion. They demonstrated that enforcing tangential boundary conditions only "in the mean" can cause significant errors for finite-length shells, and that small initial irregularities can split the bending frequency spectrum and reduce the fundamental frequency. Akhtyamov et al. [21] demonstrated that natural frequencies are highly sensitive to boundary constraints, effectively serving as a diagnostic tool for identifying specific fixing conditions. This finding underscores the importance of rigorous modeling to accurately capture the critical relationship between support constraints and the natural frequency spectrum.

Hutchinson and El-Azhari [22] devised a series of solutions for the general three-dimensional linear elasticity equations. The methodology was employed to calculate the natural frequencies of vibration for hollow elastic circular cylinders. They compared analytical results with previous finite element results. Houmat and Hutchinson [23] studied the problem using the collocation method and compared their results with previous Hutchinson model and numerical analysis results. The analytical model proposed by Ebenezer and his colleagues can be applied to axisymmetric vibrations of hollow elastic circular cylinders with arbitrary boundary conditions, whether free or fixed. It may also be used to analyze forced vibrations of cylinders whose boundaries display certain irregular displacements or stresses [24]. The study by Sharma and Sharma [25] examined the three-dimensional free vibrations in a finite-length, simply supported, homogeneous isotropic, thermally conducting circular cylinder with an eccentrically placed inner circular cavity. Grishanina and Shklyarchuk [26] applied the Riesz method to composite shells filled with liquid, revealing the significant impact of fluid inertia and ring reinforcement on modal behavior. While such variational approaches effectively handle coupled hydroelastic interactions, this complexity highlights the broader value of high-precision analytical benchmarks for understanding how boundary constraints influence fundamental frequency characteristics. Comprehensive research is ongoing into the free vibration of complex cylindrical shells. Although the Finite Element Method (FEM) is a well-known technique for analyzing the vibration of infinitely long cylindrical shells, the investigation of the impact of all the variables on the vibration response by FEM can be a time-consuming process. In engineering and in vibration phenomena, an approximate analytical solution that meets the accepted criteria for accuracy can yield valuable insights into the vibration mechanics of infinitely long cylindrical shells [27]. Singh et al. [28] integrated the Line Spring Model (LSM) with classical shell theory to analyze vibrations in cracked FGM cylinders with varying thickness. While this effectively addresses structural degradations in thin shells, exact three-dimensional solutions for healthy, thick-walled geometries remain essential to accurately distinguish between fundamental modal behaviors and the effects of such imperfections. Rawat

et al. [29] utilized the Finite Element Method (FEM) to demonstrate that end closures—such as flat, conical, or dome shapes—significantly alter the modal frequencies of thin shells. While numerical approaches effectively handle such complex geometries, parallel analytical treatments of thick-walled components provide deep physical insights that complement these finite element findings. Various analytical and numerical techniques have been applied to specific cylindrical problems. For instance, the Galerkin method was utilized by Wu and Yang [30] in three-dimensional free vibration analyses of simply supported circular hollow cylinders composed of multilayer composite and functionally graded materials. In their study, Khalili et al. [31] used the Galerkin method to investigate the free vibration problem of circular cylindrical isotropic shells simply supported or clamped on both sides. Similarly, Mofakhami et al. [32] employed the solution for infinite circular cylinders based on the separation of variables technique to derive a general solution for the vibration of finite circular cylinders. Yıldırım [33] studied one-dimensional free vibration analysis of thick-walled infinite hollow and elastic cylinders, while Hasheminejad and Ghaheri [34] examined a three-dimensional analytical model for solid elliptical cylinders. Other studies have extended these analytical approaches to complex environments, such as the free vibrations of a viscothermoelastic hollow cylinder [35]. Additionally, Aydın, and Aygün [36, 37] explored pressure-driven fluctuating laminar flow using numerical methods.

For decoupling the complex governing equations, displacement potential offers a distinct advantage. In order to separate purely shear and longitudinal motions, displacement potential functions were introduced and the translation addition theorem was employed to develop the exact solution. For instance, Ceryan and Yürüsoy [38] investigated the one-dimensional flow of non-Newtonian fluid in a pipe to determine momentum and energy equations using the general equations of motion for cylindrical coordinates. Most significantly, Atashipour et al. [39] introduced a direct approach for 3D elasto-dynamic solutions in curvilinear coordinates, utilizing a unique representation of Navier's equations to facilitate exact solutions for thick-walled cylinders. Their work demonstrates the efficiency of potential-based methods in reducing mathematical complexity without compromising the rigor of 3D elasticity theory, establishing a robust framework for analyzing frequency spectra under diverse boundary conditions. Exact analytical approaches have been effectively employed to analyze the dynamic response of cylindrical and spherical structures with various material properties [40]. Furthermore, analytical studies addressing the deformation of structural elements under specific boundary constraints have emphasized the importance of accurately modeling fixed regions [41]. Sevastyanov et al. [42] examined the coupling of torsion and circular shear in an incompressible nonlinear-elastic hollow cylinder and derived an analytical solution for a generalized neo-Hookean material. They presented a closed-form result for the Gent model, derived friction-related energy dissipation expressions, and supported the formulation with numerical–experimental comparisons for strain-softening materials, illustrating its relevance to rotary damper design. Popov et al. [43] studied axial compression of an elastic cylinder with a traction-free lateral surface, one fixed end, and a prescribed axial displacement at the other end. They proposed a refined approximate scheme that successively reduces boundary-condition discrepancies and showed, through finite element comparisons across different Poisson ratios and aspect ratios, that the approach improves analytical accuracy. Sharma et al. [44] investigated transient viscothermoelastic waves in a half-space subjected to an axisymmetric instantaneous point heat source within the Moore–Gibson–Thompson heat conduction framework. Using time-harmonic analysis and the Hankel transform, they derived expressions for the temperature, displacement, and stress fields, and validated the results against existing literature through comparisons among different thermoelasticity models. He, J. analyzed the transient thermoelastic response of an infinitely long, homogeneous isotropic hollow cylinder by incorporating both nonlocal elasticity and fractional-order thermoelasticity. Using the Laplace transform with numerical inversion, the study examined how fractional parameters, nonlocal coefficients, and time influence displacement, temperature, and stress fields, and verified the formulation by reducing to a classical case and comparing with established results [45]. Yahya et al. [46] analytically examined the harmonic magnetoelastic response of a functionally graded, orthotropic infinite cylinder with either an isotropic or a rigid core. They derived closed-form expressions for displacement and stress components and used numerical evaluations to illustrate radial stress/displacement variations, highlighting the significant influence of an applied magnetic field on the cylinder's dynamic behavior. Yu et al. [47] developed a thermo–electro–elastic coupling model for an isotropic hollow cylinder that incorporates both thermopolarization and flexoelectric effects, requiring modifications to the heat conduction, constitutive, and governing equations. Their numerical results quantified how thermopolarization and flexoelectric coefficients influence radial displacement, temperature, electric potential, and electric displacement, providing useful guidance for the design and optimization of microelectronic devices.

This study presents an in-depth investigation into the axisymmetric wave motion and vibration characteristics (governed by Navier-Lamé equations) of homogeneous and isotropic linear elastic hollow cyl-

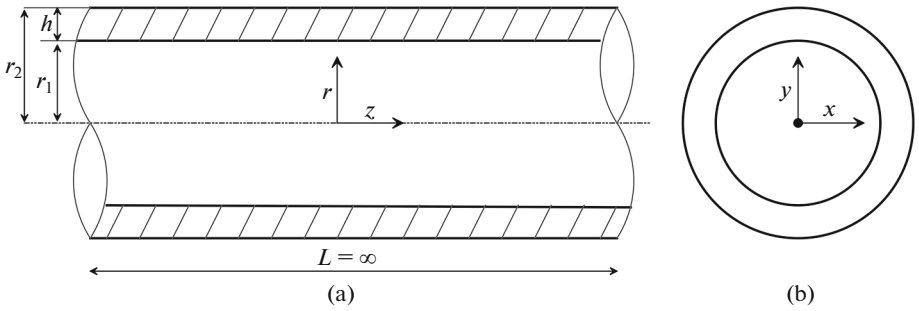

Fig. 1. (a) Cross-section of a hollow cylinder, (b) Front view of hollow cylinder.

inders fundamental components of engineering structures by employing the method of potentials to derive high-precision solutions. Developed to overcome the challenges associated with analytical solutions found in the literature, this approach comprehensively presents the dynamic behavior, natural frequencies and stress-displacement distributions of the cylinder under four distinct boundary conditions. Supported by MATLAB-based numerical analyses and dimensionless parameters, the study provides a novel dataset validated by the literature regarding cutoff frequencies and mode shapes, which are of vital importance in the design of critical structures such as pipelines and pressure vessels. This contribution serves as a significant indicator underscoring the reliability and academic value of the proposed theoretical framework.

The study is organized into four sections. The first section provides a literature review and examines existing studies. The second section details the mathematical model and the solution method employed, explaining the solution steps for each model and deriving the analytical formulas. In the third section, the analytical formulas are solved using numerical parameters and the results are presented in graphs and tables, demonstrating consistency with existing results in the literature. Finally, the fourth section evaluates and discusses the findings.

2. MATERIAL AND METHOD

The Navier-Lamé equation defines the equations of motion for a linear, homogeneous, isotropic elastic solid. A review of relevant literature reveals that the Navier-Lamé equations often resist solutions through simple methods such as separation of variables. Consequently, researchers have proposed a specialized approach known as the method of potential. In the method, the displacement vector is constructed as a combination of one or more scalar and/or vector functions, collectively termed potentials. When these representations, expressed in terms of displacement potentials, are substituted into the Navier-Lamé equations, the result is a system of partial differential equations that is either less coupled or simplified compared to the original component equations. Figure 1 illustrates a thick-walled, homogeneous, isotropic, linear, elastic hollow cylinder of infinite length. The cylinder has an inner radius of $\mathbf{r}_1$ and an outer radius of $\mathbf{r}_2$, $\mathbf{h}$ is cylinder thickness. In cylindrical coordinates, the Navier-Lamé equation can be expressed in vector form as shown in Eq. (2.1).

In a homogeneous, isotropic, linear elastic medium, the vector form of the Navier–Lamé equation (in the absence of body forces) is given as follows:

$$\mu\nabla^2\mathbf{V} + (\lambda+\mu)\nabla(\nabla\,.\mathbf{V}) = \rho\ddot{\mathbf{V}}. \tag{2.1}$$

Here,

$$\nabla^2 = \frac{\partial^2}{\partial r^2} + \frac{1}{r}\frac{\partial}{\partial r} + \frac{1}{r^2}\frac{\partial^2}{\partial\theta^2} + \frac{\partial^2}{\partial z^2}.$$

$\mathbf{V}$ denotes the displacement vector, λ and μ are the Lamé constants, ρ is the mass density, $\nabla^2\mathbf{V}$ is the vector Laplacian of the displacement vector, $\nabla\cdot\mathbf{V}$ represents the divergence of the displacement field and $\ddot{\mathbf{V}}$ denotes the second time derivative of the displacement vector.

For isotropic and homogeneous materials with Poisson's ratio ν and Young's modulus E, the Lamé constants are defined as follows.

$$\lambda = \frac{E\upsilon}{(1+\upsilon)(1-2\upsilon)}, \tag{2.2}$$

$$\mu = \frac{E}{2(1+\upsilon)}.$$

In this equation, the displacement vector **V** is written as the sum of a gradient of a scalar potential and the curl of a vector potential:

$$\mathbf{V} = \nabla\varphi + (\nabla \times \boldsymbol{\psi}), \tag{2.3}$$

where: $\varphi(r, \theta, z)$ is the scalar potential function, $\boldsymbol{\psi}(r, \theta, z)$ is the vector potential function**.**

$$\nabla\varphi = \hat{e}_r \frac{\partial\varphi}{\partial r} + \hat{e}_\theta \frac{1}{r}\frac{\partial\varphi}{\partial\theta} + \hat{e}_z \frac{\partial\varphi}{\partial z}, \tag{2.4}$$

$$\nabla \times \boldsymbol{\psi} = \left(\frac{1}{r}\frac{\partial\psi_z}{\partial\theta} - \frac{\partial\psi_\theta}{\partial z}\right)\hat{e}_r + \left(\frac{\partial\psi_r}{\partial z} - \frac{\partial\psi_z}{\partial r}\right)\hat{e}_\theta + \left(\frac{\partial\psi_\theta}{\partial r} + \frac{1}{r}\psi_\theta - \frac{1}{r}\frac{\partial\psi_r}{\partial\theta}\right)\hat{e}_z. \tag{2.5}$$

Here, $\hat{e}_r$ is radial unit vector, $\hat{e}_\theta$ is angular unit vector, $\hat{e}_z$ is axial unit vector.

By imposing an additional condition such that $\nabla \cdot \boldsymbol{\psi} = 0$ and substituting the displacement representation (2.3) into Eq. (2.1), the Navier–Lamé equation is obtained in the following form;

$$\nabla\left[(\lambda + 2\mu)\nabla^2\varphi - \rho\frac{\partial^2\varphi}{\partial t^2}\right] + \nabla \times \left[\mu\nabla^2\boldsymbol{\psi} - \rho\frac{\partial^2\boldsymbol{\psi}}{\partial t^2}\right] = 0, \tag{2.6}$$

$$\nabla \times \boldsymbol{\psi} = \left(-\frac{\partial\psi_\theta}{\partial z}\right)\hat{e}_r + \left(\frac{\partial\psi_\theta}{\partial r} + \frac{1}{r}\psi_\theta\right)\hat{e}_z. \tag{2.7}$$

In this case, the governing equation can be decomposed into two independent parts as follows;

$$C_L^2\nabla^2\varphi - \frac{\partial^2\varphi}{\partial t^2} = 0, \tag{2.8}$$

$$C_T^2\ \nabla^2\boldsymbol{\psi} - \frac{\partial^2\boldsymbol{\psi}}{\partial t^2} = 0. \tag{2.9}$$

Here,

$$C_L^2 = \frac{\lambda + 2\mu}{\rho} \quad C_T^2 = \frac{\mu}{\rho}.$$

The scalar and vector potentials are chosen as

$$\varphi = \varphi(r, z), \quad \psi_r = \psi_z = 0, \quad \psi_\theta = \psi(r, z)\mathbf{e}_\theta, \tag{2.10}$$

which is standard for axial symmetry $\left(\frac{\partial(.)}{\partial\theta} = 0\right)$ and satisfies the additional condition $\nabla \cdot \boldsymbol{\psi} = 0$. Consequently, the displacement vector is expressed as,

$$V_r = \frac{\partial\varphi}{\partial r} - \frac{\partial\psi_\theta}{\partial z}, \tag{2.11}$$

$$V_z = \frac{\partial\varphi}{\partial z} + \frac{1}{r}\frac{\partial(r\psi_\theta)}{\partial r}, \tag{2.12}$$

$$V_\theta = 0. \tag{2.13}$$

This formulation provides the fundamental components of the displacement for an axially symmetric problem. For time-harmonic wave motion along the axial direction, the potentials are assumed in the exponential form;

$$\varphi(r, z, t) = f(r)e^{i(kz-\omega t)} \tag{2.14}$$

$$\psi_\theta(r, z, t) = g(r)e^{i(kz-\omega t)} \tag{2.15}$$

Here, k, denotes the axial wave number and ω, represents the angular frequency.

By assuming Eqs. (2.14) and (2.15) are solutions of Eqs. (2.8) and (2.9), harmonic solution is sought. By using scalar function term φ in Eqs. (2.14) in Eq. (2.8) and by rearranging Eq. (2.12) is obtained;

$$\frac{d^2 f}{dr^2} + \frac{1}{r}\frac{df}{dr} + \left(\frac{\omega^2}{C_L^2} - k^2\right) f = 0. \tag{2.16}$$

The solution of ordinary differential equation (ODE) in Eq. (2.16), radial component of φ is

$$f(r) = AJ_0(pr) + BY_0(pr). \tag{2.17}$$

Here, J_0 denotes the Bessel function of the first kind of order zero and Y_0 denotes the Bessel function of the second kind (Neumann function) of order zero. A, B are constants determined from the boundary conditions. p is defined as

$$p^2 = \frac{\omega^2}{c_L^2} - k^2. \tag{2.18}$$

By substituting the vector potential $\boldsymbol{\psi}$ given in Eqs. (2.15) into Eq. (2.9) and rearranging the resulting expressions, Eq. (2.19) is obtained.

$$\frac{d^2 g}{dr^2} + \frac{1}{r}\frac{dg}{dr} + \left(\frac{\omega^2}{C_T^2} - k^2 - \frac{1}{r^2}\right) g = 0. \tag{2.19}$$

The solution of Eq. (2.19) is

$$g(r) = CJ_1(qr) + DY_1(qr). \tag{2.20}$$

Here, J_1 and Y_1 are the Bessel functions of the first and second kinds of order one, respectively. Where C, D are constants determined from the boundary conditions. q is defined as

$$q^2 = \frac{\omega^2}{c_T^2} - k^2. \tag{2.21}$$

The solutions of Eqs. (2.14) and (2.15) are

$$\varphi = \left(AJ_0(pr) + BY_0(pr)\right) e^{i(kz-\omega t)}, \tag{2.22}$$

$$\psi_\theta = \left(CJ_1(qr) + DY_1(qr)\right) e^{i(kz-\omega t)}. \tag{2.23}$$

When the displacement components V_r and V_z given in Eqs. (2.11) and (2.12) are rearranged using the potential functions provided in Eqs. (2.22) and (2.23), the following expressions are obtained.

$$V_r = \left[-ApJ_1(pr) - BpY_1(pr) - (ik)CJ_1(qr) - (ik)DY_1(qr)\right] e^{i(kz-\omega t)}, \tag{2.24}$$

$$V_z = \left[(ik)AJ_0(pr) + (ik)BY_0(pr) + CqJ_0(qr) + DqY_0(qr)\right] e^{i(kz-\omega t)}. \tag{2.25}$$

Under axisymmetric loading conditions, the strain components in cylindrical coordinates (r,θ,z) can be expressed in terms of the displacement components as follows. The axisymmetric assumption implies that the circumferential displacement is zero ($u_\theta = 0$) and that all derivatives with respect to the circumferential coordinate vanish ($\partial/\partial\theta = 0$). Assuming small displacements, the linear strain–displacement relations are given by;

$$\varepsilon_{rr} = \frac{\partial V_r}{\partial r}, \quad \varepsilon_{\theta\theta} = \frac{V_r}{r}, \quad \varepsilon_{zz} = \frac{\partial V_z}{\partial z}, \tag{2.26}$$

$$\gamma_{rz} = \frac{\partial V_r}{\partial z} + \frac{\partial V_z}{\partial r}. \tag{2.27}$$

Here, ε_{rr} denotes the radial normal strain, $\varepsilon_{\theta\theta}$ denotes the circumferential strain, ε_{zz} denotes the axial normal strain and γ_{rz} denotes the radial–axial shear strain. They are also used in the formulation of these boundary conditions and in expressing the stresses directly in terms of the displacement components.

According to Hooke's law, the stress–strain relationship for infinite cylinders made of isotropic, homogeneous and linearly elastic material is given as follows;

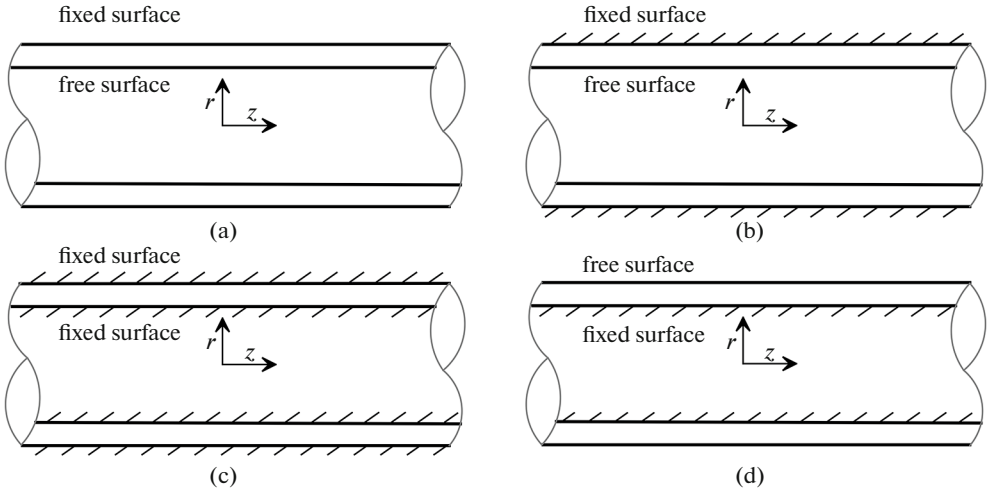

Fig. 2. Supporting models of the cylinder: (a) Free–Free support, (b) Free–Fixed support, (c) Fixed–Fixed support, (d) Fixed–Free support.

$$\sigma_{rr} = \lambda(\varepsilon_{rr} + \varepsilon_{\theta\theta} + \varepsilon_{zz}) + 2\mu\varepsilon_{rr}, \tag{2.28a}$$

$$\sigma_{\theta\theta} = \lambda(\varepsilon_{rr} + \varepsilon_{\theta\theta} + \varepsilon_{zz}) + 2\mu\varepsilon_{\theta\theta}, \tag{2.28b}$$

$$\sigma_{zz} = \lambda(\varepsilon_{rr} + \varepsilon_{\theta\theta} + \varepsilon_{zz}) + 2\mu\varepsilon_{zz}, \tag{2.28c}$$

$$\sigma_{rz} = \gamma_{rz}. \tag{2.28d}$$

Here, σ_{rr} denotes the Radial normal stress, $\sigma_{\theta\theta}$ denotes the circumferential stress, σ_{zz} denotes the axial normal stress and γ_{rz} denotes the radial–axial shear stress.

The stress components to be used in the boundary conditions are expressed directly in terms of the displacement components as follows;

$$\sigma_{rr} = \lambda\left(\frac{1}{r}\frac{\partial(rV_r)}{\partial r} + \frac{\partial V_z}{\partial z}\right) + 2\mu\frac{\partial V_r}{\partial r}, \tag{2.29}$$

$$\sigma_{rz} = \lambda\left(\frac{\partial V_z}{\partial r} + \frac{\partial V_r}{\partial z}\right). \tag{2.30}$$

If the relations given in Eqs. (2.24) and (2.25) are substituted into Eqs. (2.29) and (2.30) and rearranged, the stress components are obtained as follows;

$$\begin{aligned}\sigma_{rr} &= A\left[\left(-p^2(\underline{\lambda}+2\underline{\mu}) - \underline{\mu}k^2\right)J_0(pr) + 2\underline{\mu}\,p\frac{1}{r}J_1(pr)\right] \\ &+ B\left[\left(-p^2(\underline{\lambda}+2\underline{\mu}) - \underline{\mu}k^2\right)Y_0(pr) + 2\underline{\mu}\,p\frac{1}{r}Y_1(pr)\right] \\ &+ C\left[-2\underline{\mu}ikqJ_0(qr) + 2\underline{\mu}ik\frac{1}{r}J_1(qr)\right] + D\left[-2\underline{\mu}ikqY_0(qr) + 2\underline{\mu}ik\frac{1}{r}Y_1(qr)\right],\end{aligned} \tag{2.31}$$

$$\begin{aligned}\sigma_{rz} &= A\left[-2\underline{\mu}ikpJ_1(pr)\right] + B\left[-2\underline{\mu}ikpY_1(pr)\right] \\ &+ C\left[\underline{\mu}\left(k^2-q^2\right)J_1(qr)\right] + D\left[\underline{\mu}\left(k^2-q^2\right)Y_1(qr)\right].\end{aligned} \tag{2.32}$$

In this study, four different models are considered for the hollow cylinder, each characterized by its own specific boundary conditions (Fig. 2).

Free–Free: Both the inner and outer surfaces of the cylinder are traction-free. Therefore, the radial and radial–axial shear stresses vanish at both the inner radius $r = a$ and the outer radius $r = b$ (Fig. 2a).

at $r = a$ and $r = b$; $\sigma_{rr} = 0, \quad \sigma_{rz} = 0.$

Table 1. Models, boundary conditions, the physical meanings and typical engineering applications

Model	Boundary condition at $r = a$	Boundary condition at $r = b$	Physical meaning	Typical applications
Free–Free	$\sigma_{rr} = 0$ $\sigma_{rz} = 0$	$\sigma_{rr} = 0$ $\sigma_{rz} = 0$	Both ends are free of traction; no support	Free vibration analysis of long pipes; laboratory experiments; unconstrained cylinders
Fixed–Free	$V_r = 0$ $V_z = 0$	$\sigma_{rr} = 0$ $\sigma_{rz} = 0$	One end fixed, other end free	Cantilever beams; single-supported cylinders; vibration analysis of partially supported elements
Fixed–Fixed	$V_r = 0$ $V_z = 0$	$V_r = 0$ $V_z = 0$	One end fixed, other end fixed	Pipes with both ends fixed; pressure vessels; structural elements with fixed supports
Free–Fixed	$\sigma_{rr} = 0$ $\sigma_{rz} = 0$	$V_r = 0$ $V_z = 0$	One end free, other end fixed	Single-supported cylinders; cantilever-like structures; vibration studies of partially constrained elements

Fixed–Free: The inner end of the cylinder surface is fixed, meaning both radial and axial displacements are zero ($V_r = V_z = 0$), while the outer end is free, so the radial and shear stresses vanish (Fig. 2d).

$$\text{at } r = a; \quad V_r = 0, \quad V_z = 0,$$
$$\text{at } r = b; \quad \sigma_{rr} = 0, \quad \sigma_{rz} = 0.$$

Fixed–Fixed: Both ends of the cylinder are fixed, resulting in zero displacements at $r = a$ and $r = b$ (Fig. 2c).

at $r = a$ and $r = b$; $V_r = 0, \quad V_z = 0$.

Free–Fixed: The inner end is free, so the radial and shear stresses vanish ($\sigma_{rr} = \sigma_{rz} = 0$), while the outer end is fixed, with zero radial and axial displacements (Fig. 2b).

$$\text{at } r = a; \quad \sigma_{rr} = 0, \quad \sigma_{rz} = 0,$$
$$\text{at } r = b; \quad V_r = 0, \quad V_z = 0.$$

These boundary conditions are applied to model various support scenarios and are essential for the formulation of the governing equations of the hollow cylinder (Eqs. 2.24, 2.25 and 2.31, 2.32). The physical meanings, constraints and typical engineering applications of the models are summarized in Table 1.

In all models, characteristic equations giving the eigen angular frequency are obtained when the boundary conditions are applied; Accordingly,

From Eqs. (2.31) and (2.32);

at $r = a$:

$$\begin{aligned}\sigma_{rz} = 0 \Rightarrow\ & A\left[-2ikpJ_1(pa)\right] + B\left[-2ikpY_1(pa)\right] \\ & + C\left[-\left(q^2 - k^2\right)J_1(qa)\right] + D\left[-\left(q^2 - k^2\right)Y_1(qa)\right] = 0,\end{aligned} \tag{2.33}$$

$$\begin{aligned}\sigma_{rr} = 0 \Rightarrow\ & A\left[-\frac{1}{2}\left(q^2 - k^2\right)J_0(pa) + p\frac{1}{a}J_1(pa)\right] + B\left[-\frac{1}{2}\left(q^2 - k^2\right)Y_0(pa) + p\frac{1}{a}Y_1(pa)\right] \\ & + C\left[-ikqJ_0(qa) + ik\frac{1}{a}J_1(qa)\right] + D\left[-ikqY_0(qa) + ik\frac{1}{a}Y_1(qa)\right] = 0\end{aligned} \tag{2.34}$$

at $r = b$:

$$\begin{aligned}\sigma_{rz} = 0 \Rightarrow\ & A\left[-2ikpJ_1(pb)\right] + B\left[-2ikpY_1(pb)\right] + C\left[-\left(q^2 - k^2\right)J_1(qb)\right] \\ & + D\left[-\left(q^2 - k^2\right)Y_1(qb)\right] = 0,\end{aligned} \tag{2.35}$$

$$\sigma_{rr} = 0 \Rightarrow A\left[-\frac{1}{2}\left(q^2 - k^2\right)J_0(pb) + p\frac{1}{b}J_1(pb)\right] + B\left[-\frac{1}{2}\left(q^2 - k^2\right)Y_0(pb) + p\frac{1}{b}Y_1(pb)\right] + C\left[-ikqJ_0(qb) + ik\frac{1}{b}J_1(qb)\right] + D\left[-ikqY_0(qb) + ik\frac{1}{b}Y_1(qb)\right] = 0. \tag{2.36}$$

From Eqs. (2.24) and (2.25);

at $r = a$:

$$V_r = 0 \Rightarrow \left[-ApJ_1(pa) - BpY_1(pa) - (ik)CJ_1(qa) - (ik)DY_1(qa)\right] = 0, \tag{2.37}$$

$$V_z = 0 \Rightarrow \left[(ik)AJ_0(pa) + (ik)BY_0(pa) + CqJ_0(qa) + DqY_0(qa)\right] = 0, \tag{2.38}$$

at $r = b$:

$$V_r = 0 \Rightarrow \left[-ApJ_1(pb) - BpY_1(pb) - (ik)CJ_1(qb) - (ik)DY_1(qb)\right] = 0, \tag{2.39}$$

$$V_z = 0 \Rightarrow \left[(ik)AJ_0(pb) + (ik)BY_0(pb) + CqJ_0(qb) + DqY_0(qb)\right] = 0. \tag{2.40}$$

For Free–Free, Eqs. (2.33), (2.34), (2.35), and (2.36), which are obtained based on the boundary conditions, will be used.

For Fixed–Free, Eqs. (2.35), (2.36), (2.37), and (2.38), which are obtained based on the boundary conditions, will be used.

For Fixed–Fixed, Eqs. (2.37), (2.38), (2.39), and (2.40), which are obtained based on the boundary conditions, will be used.

For Free–Fixed, Eqs. (2.33), (2.34), (2.39), and (2.40), which are obtained based on the boundary conditions, will be used.

Dimensionless

$$r_1 = a, \quad r_2 = b, \quad s = \frac{a}{b}, \quad h = b - a, \quad b = h\frac{1}{(1-s)},$$

$$a = h\frac{s}{(1-s)},$$

$$\Omega = \frac{\omega h}{C_T}, \quad \xi = kh,$$

$$x^2 = (qh)^2 = \Omega^2 - \xi^2, \quad \gamma^2 = \frac{C_L^2}{C_T^2} = \frac{2(1-\upsilon)}{1-2\upsilon}, \quad y^2 = (ph)^2 = \gamma^{-2}\Omega^2 - \xi^2. \tag{2.41}$$

The obtained dimensional equations (Eqs. (2.33), (2.34), (2.35), (2.36), (2.37), (2.38), (2.39), and (2.40)) have been rendered dimensionless by employing the dimensionless parameters and variables defined in Eq. (2.41). For each proposed model, a linear homogeneous system of equations expressed in terms of the coefficients A, B, C, and D has been constructed separately (the corresponding equations for each model are provided in the Appendix). This system constitutes an algebraic eigenvalue problem for the angular frequency. The matrix form of this linear homogeneous system of equations is given below as Eq. (2.42).

$$\begin{bmatrix} K_{11} & K_{12} & K_{13} & K_{14} \\ K_{21} & K_{22} & K_{23} & K_{24} \\ K_{31} & K_{32} & K_{33} & K_{34} \\ K_{41} & K_{42} & K_{43} & K_{44} \end{bmatrix} \begin{bmatrix} A \\ B \\ C \\ D \end{bmatrix} = \begin{bmatrix} 0 \\ 0 \\ 0 \\ 0 \end{bmatrix}. \tag{2.42}$$

For each model, the elements of the obtained coefficient matrix are presented in Table 2.

In order to obtain a non-zero solution of the homogeneous equation set, it is necessary to set the determinant of the (4 × 4) dimensional coefficients matrix equal to zero. This condition is the characteristic equation that gives the eigenvalue angular frequency. This characteristic equation is a function of dimensionless wave number (ξ) and angular frequency (Ω). This characteristic equation is a function of the dimensionless wave number (ξ) and angular frequency (Ω) defined in Eq. (2.41).

Table 2. For each model, the elements of the obtained coefficient matrix

	Free−Free	Fixed−Free	Fixed−Fixed	Free−Fixed
K_{11}	$\left[-\frac{1}{2}\left(x^2-\xi^2\right)J_0\left(y\frac{s}{(1-s)}\right)+\frac{y(1-s)}{s}J_1\left(y\frac{s}{(1-s)}\right)\right]$	$\left[-\frac{1}{2}\left(x^2-\xi^2\right)J_0\left(y\frac{1}{(1-s)}\right)+y(1-s)J_1\left(y\frac{s}{(1-s)}\right)\right]$	$\left[yJ_1\left(y\frac{s}{(1-s)}\right)\right]$	$\left[-\frac{1}{2}\left(x^2-\xi^2\right)J_0\left(y\frac{s}{(1-s)}\right)+\frac{y(1-s)}{s}J_1\left(y\frac{s}{(1-s)}\right)\right]$
K_{12}	$\left[-\frac{1}{2}\left(x^2-\xi^2\right)Y_0\left(y\frac{s}{(1-s)}\right)+\frac{y(1-s)}{s}Y_1\left(y\frac{s}{(1-s)}\right)\right]$	$\left[-\frac{1}{2}\left(x^2-\xi^2\right)Y_0\left(y\frac{1}{(1-s)}\right)+y(1-s)Y_1\left(y\frac{s}{(1-s)}\right)\right]$	$\left[yY_1\left(y\frac{s}{(1-s)}\right)\right]$	$\left[-\frac{1}{2}\left(x^2-\xi^2\right)Y_0\left(y\frac{s}{(1-s)}\right)+\frac{y(1-s)}{s}Y_1\left(y\frac{s}{(1-s)}\right)\right]$
K_{13}	$\left[-i\xi xJ_0\left(x\frac{s}{(1-s)}\right)+i\frac{\xi(1-s)}{s}J_1\left(x\frac{s}{(1-s)}\right)\right]$	$\left[-i\xi xJ_0\left(x\frac{1}{(1-s)}\right)+i\xi(1-s)J_1\left(x\frac{1}{(1-s)}\right)\right]$	$\left[i\xi J_1\left(x\frac{s}{(1-s)}\right)\right]$	$\left[-i\xi xJ_0\left(x\frac{s}{(1-s)}\right)+i\frac{\xi(1-s)}{s}J_1\left(x\frac{s}{(1-s)}\right)\right]$
K_{14}	$\left[-i\xi xY_0\left(x\frac{s}{(1-s)}\right)+i\frac{\xi(1-s)}{s}Y_1\left(x\frac{s}{(1-s)}\right)\right]$	$\left[-i\xi xY_0\left(x\frac{1}{(1-s)}\right)+i\xi(1-s)Y_1\left(x\frac{1}{(1-s)}\right)\right]$	$\left[i\xi Y_1\left(x\frac{s}{(1-s)}\right)\right]$	$\left[-i\xi xY_0\left(x\frac{s}{(1-s)}\right)+i\frac{\xi(1-s)}{s}Y_1\left(x\frac{s}{(1-s)}\right)\right]$
K_{21}	$\left[-\frac{1}{2}\left(x^2-\xi^2\right)J_0\left(y\frac{1}{(1-s)}\right)+y(1-s)J_1\left(y\frac{1}{(1-s)}\right)\right]$	$\left[-2i\xi yJ_1\left(y\frac{1}{(1-s)}\right)\right]$	$\left[i\xi J_0\left(y\frac{s}{(1-s)}\right)\right]$	$\left[-2i\xi yJ_1\left(y\frac{s}{(1-s)}\right)\right]$
K_{22}	$\left[-\frac{1}{2}\left(x^2-\xi^2\right)Y_0\left(y\frac{1}{(1-s)}\right)+y(1-s)Y_1\left(y\frac{1}{(1-s)}\right)\right]$	$\left[-2i\xi yY_1\left(y\frac{1}{(1-s)}\right)\right]$	$\left[i\xi Y_0\left(y\frac{s}{(1-s)}\right)\right]$	$\left[-2i\xi yY_1\left(y\frac{s}{(1-s)}\right)\right]$
K_{23}	$\left[-i\xi xJ_0\left(x\frac{1}{(1-s)}\right)+i\xi(1-s)J_1\left(x\frac{1}{(1-s)}\right)\right]$	$\left[-\left(x^2-\xi^2\right)J_1\left(x\frac{1}{(1-s)}\right)\right]$	$\left[xJ_0\left(x\frac{s}{(1-s)}\right)\right]$	$\left[-\left(x^2-\xi^2\right)J_1\left(x\frac{s}{(1-s)}\right)\right]$
K_{24}	$\left[-i\xi xY_0\left(x\frac{1}{(1-s)}\right)+i\xi(1-s)Y_1\left(x\frac{1}{(1-s)}\right)\right]$	$\left[-\left(x^2-\xi^2\right)Y_1\left(x\frac{1}{(1-s)}\right)\right]$	$\left[xY_0\left(x\frac{s}{(1-s)}\right)\right]$	$\left[-\left(x^2-\xi^2\right)Y_1\left(x\frac{s}{(1-s)}\right)\right]$
K_{31}	$\left[-2i\xi yJ_1\left(y\frac{s}{(1-s)}\right)\right]$	$\left[yJ_1\left(y\frac{s}{(1-s)}\right)\right]$	$\left[yJ_1\left(y\frac{1}{(1-s)}\right)\right]$	$\left[yJ_1\left(y\frac{1}{(1-s)}\right)\right]$
K_{32}	$\left[-2i\xi yY_1\left(y\frac{s}{(1-s)}\right)\right]$	$\left[yY_1\left(y\frac{s}{(1-s)}\right)\right]$	$\left[yY_1\left(y\frac{1}{(1-s)}\right)\right]$	$\left[yY_1\left(y\frac{1}{(1-s)}\right)\right]$
K_{33}	$\left[-\left(x^2-\xi^2\right)J_1\left(x\frac{s}{(1-s)}\right)\right]$	$\left[i\xi J_1\left(x\frac{s}{(1-s)}\right)\right]$	$\left[i\xi J_1\left(x\frac{1}{(1-s)}\right)\right]$	$\left[i\xi J_1\left(x\frac{1}{(1-s)}\right)\right]$
K_{34}	$\left[-\left(x^2-\xi^2\right)Y_1\left(x\frac{s}{(1-s)}\right)\right]$	$\left[i\xi Y_1\left(x\frac{s}{(1-s)}\right)\right]$	$\left[i\xi Y_1\left(x\frac{1}{(1-s)}\right)\right]$	$\left[i\xi Y_1\left(x\frac{1}{(1-s)}\right)\right]$

Table 2. (Contd.)

	Free–Free	Fixed–Free	Fixed–Fixed	Free–Fixed
K_{41}	$\left[-2i\xi y J_1\left(y\frac{1}{(1-s)}\right)\right]$	$\left[i\xi J_0\left(y\frac{s}{(1-s)}\right)\right]$	$\left[i\xi J_0\left(y\frac{1}{(1-s)}\right)\right]$	$\left[i\xi J_0\left(y\frac{1}{(1-s)}\right)\right]$
K_{42}	$\left[-2i\xi y Y_1\left(y\frac{1}{(1-s)}\right)\right]$	$\left[i\xi Y_0\left(y\frac{s}{(1-s)}\right)\right]$	$\left[i\xi Y_0\left(y\frac{1}{(1-s)}\right)\right]$	$\left[i\xi Y_0\left(y\frac{1}{(1-s)}\right)\right]$
K_{43}	$\left[-\left(x^2-\xi^2\right)J_1\left(x\frac{1}{(1-s)}\right)\right]$	$\left[i\xi Y_0\left(y\frac{s}{(1-s)}\right)\right]$	$\left[xJ_0\left(x\frac{1}{(1-s)}\right)\right]$	$\left[xJ_0\left(x\frac{1}{(1-s)}\right)\right]$
K_{44}	$\left[-\left(x^2-\xi^2\right)Y_1\left(x\frac{1}{(1-s)}\right)\right]$	$\left[xY_0\left(x\frac{s}{(1-s)}\right)\right]$	$\left[xY_0\left(x\frac{1}{(1-s)}\right)\right]$	$\left[xY_0\left(x\frac{1}{(1-s)}\right)\right]$

3. RESULTS AND DISCUSSION

The system of equations obtained from Eq. (2.42) was solved numerically based on the analytical formulation. In this study, the Poisson's ratio of the cylindrical rod was taken as $\nu = 0.3$, and the geometric ratio was assumed as $s = a/b = 0.5$. Numerical computations were carried out using MATLAB software tools. To obtain the natural frequencies and dissipation factors, an eigenvalue solution approach based on the numerical determination of the roots of the characteristic equation derived from the governing equation system was employed. In this study, the frequency values that make the determinant of the coefficient matrix equal to zero were sought.

In the method, the algebraic equation system obtained by applying the boundary conditions (Eq. (2.42)) is written in the form of a coefficient matrix. For the system to have a non-trivial solution, the determinant of this matrix must be equal to zero. In the literature, different numerical techniques such as the Newton–Raphson method, secant method, bisection algorithm, and shooting method are used to determine the eigenfrequencies that make the determinant zero. In this study, the shooting method was preferred. In this way, convergence was accelerated by using different step intervals.

The shooting method is used as an optimization algorithm in various mathematical problems [48, 49]. First, initial values are estimated for the parameters to be optimized. Then, problem-specific constraint conditions (such as integral relations, determinants, or equation systems) are evaluated and compared with known values. Based on the resulting error values, new estimates of the initial parameters that satisfy the constraint conditions are generated. This procedure is repeated iteratively until the constraint conditions are satisfied with the desired level of accuracy. A more detailed discussion of the shooting method is provided in [50–52], which present comprehensive explanations for different application areas. The mathematical formulation of the shooting method is given in the Appendix section.

Thus, the frequency values satisfying the boundary conditions correspond to the natural frequencies of the system, while the complex solutions represent the dissipation factors. In order to increase the accuracy of the numerical solution, the initial values were defined over a wide solution interval and the solution procedure was carried out accordingly. Starting from different initial points, the solutions converge to certain numerical values. These convergence values provide the different eigenvalues required for the solution of the problem. Once the eigenvalues are obtained, new initial guesses are defined around the existing eigenvalues and convergence is achieved with smaller tolerance values (e.g., 10^{-6}, 10^{-8}).

When the dimensionless wave number (ξ) is equal to zero, no wave propagation occurs. The dimensionless angular frequency (Ω) values at this point correspond to the cut-off frequencies. Below these frequencies, the system cannot support wave propagation. Therefore, to determine the frequency range in which wave propagation can occur, the dimensionless wave number was taken as $\xi = 0$, and the cut-off frequencies for the four proposed models were calculated in the MATLAB environment. The obtained values are presented in Table 3.

In the Free–Free model, both the inner and outer surfaces of the cylinder are free. Since the stresses vanish on both surfaces, the system has the minimum constraint, and therefore the cut-off frequencies take the lowest values. In the Free–Fixed model, the outer surface is fixed. This increases the stiffness of the system and leads to higher cut-off frequencies. In the Fixed–Free model, the inner surface is fixed. The constraint on the inner surface limits the deformation field more significantly; therefore, the effective stiffness of the system is generally slightly greater than that of the Free–Fixed case, resulting in higher cut-

Table 3. Cut-off frequencies for thick-walled cylinders ($\nu = 0.3$, $s = a/b = 0.5$)

Free–Free	Free–Fixed	Fixed–Fixed	Fixed–Free
1.1847	1.3608	3.1230	1.7940
3.1966	4.6459	6.2734	4.8021
6.3123	7.8142	9.4182	7.9090
9.4445	10.9671	12.5614	11.0351
12.5812	14.1151	15.7040	14.1680
15.7199	17.2607	18.8462	17.3040
18.8595	20.4050	21.9883	20.4417
21.9997	23.5487	25.1303	23.5805
25.1402	26.4682	28.2721	26.4826
28.2810	29.8347	31.4139	29.8598

off frequencies. In the Fixed–Fixed model, both surfaces are fixed, meaning that the deformation is most strongly constrained. Consequently, the system possesses the maximum stiffness, and the cut-off frequencies reach their highest values.

In Fig. 3, the variation of the dimensionless angular frequency (Ω) with respect to the dimensionless wave number (ξ) is presented by considering the first eight vibration modes. Each graph illustrates the dispersion curves corresponding to the first eight modes for the four proposed models.

As seen in Fig. 3, for all models the dimensionless angular frequency (Ω) generally increases as the dimensionless wave number (ξ) increases. This behavior indicates that cylindrical shell waves exhibit a characteristic positive dispersive behavior. In particular, the slope of the frequency increase is more pronounced in the lower modes (Modes 1–3). In contrast, for higher modes (Modes 6–8), the curves tend to become nearly horizontal. Physically, this behavior can be explained by the fact that the lower modes represent the global deformation characteristics of the system and are therefore more strongly influenced by the boundary conditions. In higher modes, however, the deformation becomes more localized, reducing the influence of the boundary conditions and resulting in dispersion curves with a weaker slope.

Considering the cut-off frequencies given in Table 3 and the intersections at $\xi = 0$ in Fig. 3, it is clearly observed that the first model (Free–Free) possesses the lowest cut-off frequencies. This result is physically consistent because the free–free boundary condition allows rotation while restricting displacement, leading to a lower bending stiffness compared to clamped conditions. In contrast, in models containing

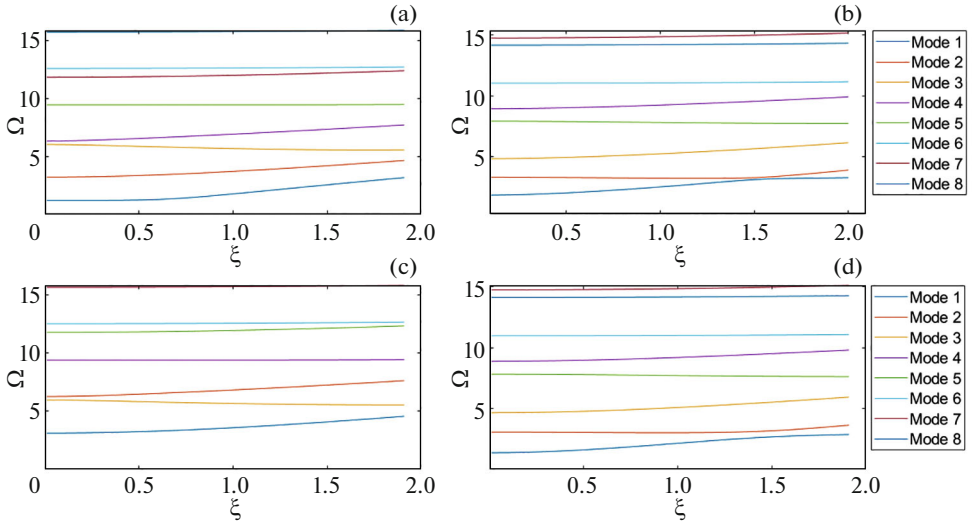

Fig. 3. Variation of dimensionless wave number (ξ) and dimensionless angular frequency (Ω), (a) Free–Free, (b) Fixed–Free, (c) Fixed–Fixed, (d) Free–Fixed.

clamped edges, both displacement and rotation are constrained, which increases the overall stiffness of the system and consequently leads to higher cut-off frequencies. Although small numerical differences exist between the Fixed–Free and Free–Fixed models, the dispersion curves exhibit very similar characteristics. The main reason for this similarity is that both models contain one clamped and one free edge, resulting in a largely similar global stiffness distribution of the system. The small differences observed can be attributed to asymmetric kinematic effects arising from the opposite axial positioning of the boundary conditions.

Thus, the graphs obtained in Fig. 3 demonstrate that boundary conditions play a decisive role particularly in determining the cut-off frequencies and the behavior of the lower modes. However, as the mode number increases, the influence of the boundary conditions gradually decreases.

In Fig. 4, the radial displacement distributions of the cylinder along the thickness direction under different boundary conditions are presented. In the graphs, the horizontal axis represents the radius (r), while the vertical axis denotes the radial displacement (V_r). In Fig. 4a, corresponding to the Free–Free model, there is no constraint imposed on the displacement. Therefore, the displacement field is normalized in order to eliminate the effect of rigid body motion. Since both the inner and outer surfaces of the cylinder are traction-free, the displacement distribution varies more freely and smoothly along the thickness. In Fig. 4b, which represents the Free–Fixed case, the inner surface is free while the outer surface is fixed. As a result, the displacement distribution exhibits an asymmetric character, and the deformation becomes more pronounced near the free surface. In Fig. 4c, corresponding to the Fixed–Fixed model, both surfaces are constrained. Consequently, the displacement becomes zero at the boundary surfaces, and the maximum deformation occurs in the middle region of the cylinder thickness. This behavior arises because the constraints at the boundaries restrict motion, causing the deformation to concentrate within the interior region. In Fig. 4d, representing the Fixed–Free case, the inner surface is fixed while the outer surface is free. Therefore, the displacement distribution again shows an asymmetric character, with the deformation increasing toward the free surface. In general, the increasing restrictive effect of the boundary conditions enhances the stiffness of the system, and accordingly, the character of the displacement distribution changes significantly.

In Figure 5, the radial stress distributions of the cylinder along the thickness direction under different boundary conditions are presented. In the graphs, the horizontal axis represents the radius (r), while the vertical axis denotes the radial stress (σ_r). In Fig. 5a, corresponding to the Free–Free boundary condition, both the inner and outer surfaces are traction-free. Therefore, the radial stress values approach zero near the surfaces, while the maximum stresses occur in the middle region of the cylinder thickness. This behavior is associated with the fact that the structure is unconstrained on both sides, allowing the deformation to develop more freely throughout the thickness. In the Free–Fixed (Fig. 5b) and Fixed–Free (Fig. 5d) boundary conditions, the fixation of only one surface makes the deformation field asymmetric and causes the stress distribution to vary irregularly along the cylinder thickness. Since the displacement is restricted at the fixed surface, stress gradients become more pronounced in this region, whereas the stresses decrease toward the free surface. In the Fixed–Fixed model (Fig. 5c), both surfaces are constrained. As a result, the structural restriction increases, leading to a stronger limitation of the deformation. Consequently, the stress distribution exhibits higher amplitudes and more pronounced oscillations.

The obtained stress distributions are also consistent with results reported in the literature on the elasto-dynamic behavior of cylindrical structures. In analytical solutions of wave propagation and vibration problems in cylindrical coordinate systems, it is well known that displacement and stress fields are generally expressed in terms of Bessel functions. For this reason, the stress distributions exhibit an oscillatory character along the cylinder thickness, leading to the formation of certain nodal and peak points. In particular, under free surface conditions, the radial stress is forced to vanish at the boundary surfaces, which causes the stress field to redistribute toward the interior regions of the cross-section. In contrast, fixed boundary conditions restrict displacements, thereby limiting the deformation field and causing stress gradients to concentrate in specific regions along the thickness. Classical studies on the elasto-dynamic analysis of cylindrical shells and thick cylinders show that maximum stresses often occur at a certain distance from the surfaces, typically near the middle region of the cylinder thickness. This behavior can be explained as a natural consequence of the vibration modes generated by wave propagation in the thickness direction of cylindrical structures. The results obtained in this study are consistent with this theoretical expectation and demonstrate that different boundary conditions have a significant influence on the stress amplitude and distribution characteristics. This finding is also in agreement with trends reported in the literature concerning elastic wave propagation and vibration behavior in cylindrical structures [5, 6].

Table 4 presents a comparison of the eigenvalues obtained for thick-walled cylinders under Free–Free boundary conditions with those reported in several studies in the literature. The eigenvalues obtained in

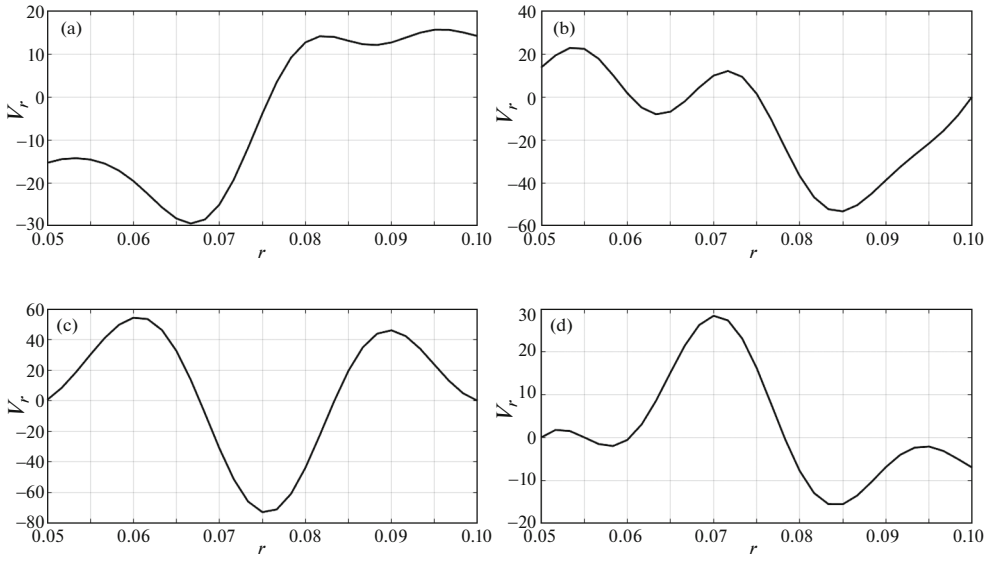

Fig. 4. Radial displacement distributions through the thickness of the cylinder for different support models: (a) Free–Free, (b) Free–Fixed, (c) Fixed–Fixed, (d) Fixed–Free.

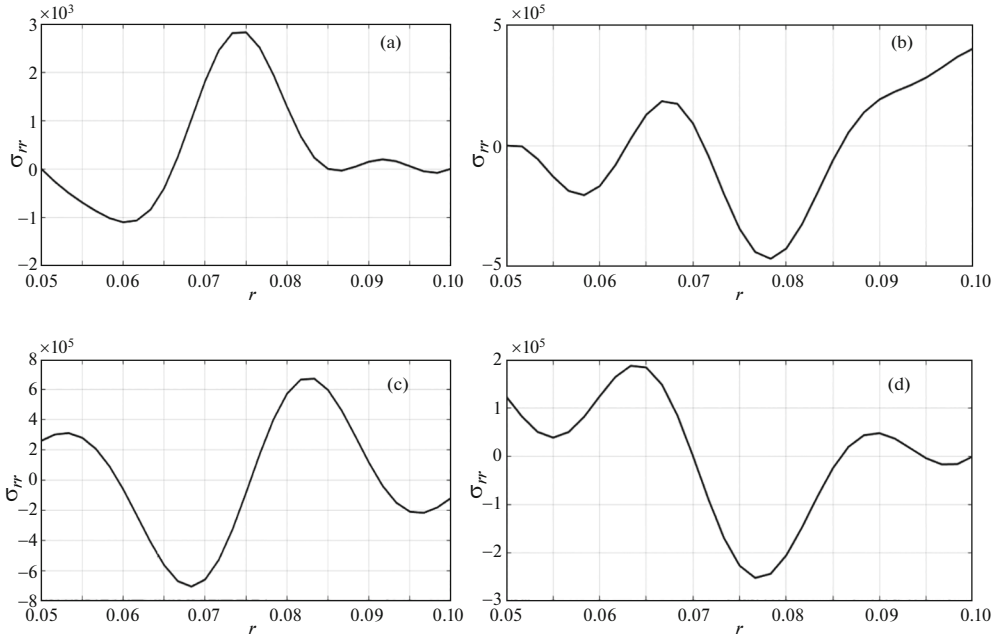

Fig. 5. Radial stress distributions across the thickness of the cylinder for different boundary condition models: (a) Free–Free, (b) Free–Fixed, (c) Fixed–Fixed, (d) Fixed–Free.

the present study show very good agreement with the results reported by Houmat [23], Hasheminejad [34], and Keles [40]. In particular, it can be observed that the differences between the values for all modes are very small and that the results are of the same order of magnitude. This agreement confirms the accuracy and reliability of the mathematical model used as well as the numerical solution method applied in this study. Furthermore, it is observed that the eigenvalues increase regularly with increasing mode number, which is consistent with the vibration theory of cylindrical structures. Therefore, the comparison presented in Table 4 demonstrates that the numerical method employed in the present study is consistent with the results reported in the literature and that the developed model can be reliably used for the vibration analysis of thick-walled cylinders.

Table 4. Comparison of Eigenvalues Obtained for Thick-Walled Cylinders with "Free-Free Ends" in [23], [34], [40] ($\nu = 0.3$, $s = a/b = 0.5$)

Current study	Ref. [23]	Ref. [34]	Ref. [40]
3.1966	3.21655	3.218	3.21793
6.3123	6.3193	6.319	6.31999
9.4445	9.44864	9.449	9.44910
12.5812	12.5842	12.58	12.58455
15.7199	15.7222	15.72	15.72249
18.8595	18.8614	18.86	18.86165
21.9997	22.0013	22.00	22.00151
25.1402	25.1416	25.14	25.14180
28.2810	28.2822	28.28	28.28239

4. CONCLUSIONS

In this study, the wave propagation and vibration behavior of a thick-walled cylinder were numerically investigated under different boundary conditions. The governing equations obtained in cylindrical coordinates were solved under appropriate boundary conditions, and the dynamic characteristics of the system were determined. Based on the obtained results, the following main conclusions can be drawn:

1. It was observed that the dynamic behavior of the cylinder strongly depends on the boundary conditions. Under the Free–Free boundary condition, the system has lower stiffness; therefore, the cut-off frequencies were found to be smaller compared to those of the other boundary conditions.

2. In models with fixed boundary conditions (Free–Fixed, Fixed–Fixed, and Fixed–Free), the stiffness of the structure increases, and accordingly, higher natural frequencies are obtained. In particular, the highest frequency values were observed in the Fixed–Fixed model.

3. Examination of the radial displacement distributions shows that the deformation is larger and more smoothly distributed at free surfaces, whereas the displacements are significantly restricted at fixed surfaces. This indicates that boundary conditions directly affect the deformation characteristics.

4. The stress distributions reveal that in cases with fixed boundary conditions, the stress gradients increase and stress concentrations occur particularly near the boundary regions.

5. The obtained eigenvalues were compared with results reported in the literature, and a very good agreement was observed. This confirms the accuracy of the developed mathematical model and the numerical solution method used in the study.

In conclusion, the results demonstrate that boundary conditions play an important role in determining the wave propagation and vibration characteristics of thick-walled cylinders. The findings obtained in this study are expected to provide a useful reference for the dynamic analysis of cylindrical structures, pipe systems, and similar engineering applications.

APPENDIX

For each model, the system of equations obtained as a result of the nondimensionalization process is given below;

Free-Free Model

By rearranging Eqs. (2.33), (2.34), (2.35), and (2.36) obtained for free-free model using dimensionless parameters and variables, the following equations are obtained.

$$A\left[-2i\frac{\xi y}{h^2}J_1\left(y\frac{s}{(1-s)}\right)\right]+B\left[-2i\frac{\xi y}{h^2}Y_1\left(y\frac{s}{(1-s)}\right)\right]$$

$$+C\left[-\left(x^2-\xi^2\right)\frac{1}{h^2}J_1\left(x\frac{s}{(1-s)}\right)\right]+D\left[-\left(x^2-\xi^2\right)\frac{1}{h^2}Y_1\left(x\frac{s}{(1-s)}\right)\right]=0, \quad \text{(A.1)}$$

$$A\left[-\frac{1}{2}\left(\frac{x^2-\xi^2}{h^2}\right)J_0\left(y\frac{s}{(1-s)}\right)+\frac{y(1-s)}{h^2 s}J_1\left(y\frac{s}{(1-s)}\right)\right]$$
$$+B\left[-\frac{1}{2}\left(\frac{x^2-\xi^2}{h^2}\right)Y_0\left(y\frac{s}{(1-s)}\right)+\frac{y(1-s)}{h^2 s}Y_1\left(y\frac{s}{(1-s)}\right)\right]$$
$$+C\left[-i\frac{\xi x}{h^2}J_0\left(x\frac{s}{(1-s)}\right)+i\frac{\xi(1-s)}{h^2 s}J_1\left(x\frac{s}{(1-s)}\right)\right]$$
$$+D\left[-i\frac{\xi x}{h^2}Y_0\left(x\frac{s}{(1-s)}\right)+i\frac{\xi(1-s)}{h^2 s}Y_1\left(x\frac{s}{(1-s)}\right)\right]=0, \tag{A.2}$$

$$A\left[-2i\frac{\xi y}{h^2}J_1\left(y\frac{1}{(1-s)}\right)\right]+B\left[-2i\frac{\xi y}{h^2}Y_1\left(y\frac{1}{(1-s)}\right)\right]$$
$$+C\left[-\left(x^2-\xi^2\right)\frac{1}{h^2}J_1\left(x\frac{1}{(1-s)}\right)\right]+D\left[-\left(x^2-\xi^2\right)\frac{1}{h^2}Y_1\left(x\frac{1}{(1-s)}\right)\right]=0, \tag{A.3}$$

$$A\left[-\frac{1}{2}\left(\frac{x^2-\xi^2}{h^2}\right)J_0\left(y\frac{1}{(1-s)}\right)+\frac{y(1-s)}{h^2}J_1\left(y\frac{1}{(1-s)}\right)\right]$$
$$+B\left[-\frac{1}{2}\left(\frac{x^2-\xi^2}{h^2}\right)Y_0\left(y\frac{1}{(1-s)}\right)+\frac{y(1-s)}{h^2}Y_1\left(y\frac{1}{(1-s)}\right)\right]$$
$$+C\left[-i\frac{\xi x}{h^2}J_0\left(x\frac{1}{(1-s)}\right)+i\frac{\xi(1-s)}{h^2}J_1\left(x\frac{1}{(1-s)}\right)\right]$$
$$+D\left[-i\frac{\xi x}{h^2}Y_0\left(x\frac{1}{(1-s)}\right)+i\frac{\xi(1-s)}{h^2}Y_1\left(x\frac{1}{(1-s)}\right)\right]=0. \tag{A.4}$$

Fixed-Free Model

By rearranging Eqs. (A.2.35), (A.2.36), (A.2.37), and (A.2.38) obtained for fixed-free model using dimensionless parameters and variables, the following equations are obtained.

$$A\left[-2i\frac{\xi y}{h^2}J_1\left(y\frac{1}{(1-s)}\right)\right]+B\left[-2i\frac{\xi y}{h^2}Y_1\left(y\frac{1}{(1-s)}\right)\right]$$
$$+C\left[-\left(x^2-\xi^2\right)\frac{1}{h^2}J_1\left(x\frac{1}{(1-s)}\right)\right]+D\left[-\left(x^2-\xi^2\right)\frac{1}{h^2}Y_1\left(x\frac{1}{(1-s)}\right)\right]=0, \tag{A.5}$$

$$A\left[-\frac{1}{2}\left(\frac{x^2-\xi^2}{h^2}\right)J_0\left(y\frac{1}{(1-s)}\right)+\frac{y(1-s)}{h^2}J_1\left(y\frac{1}{(1-s)}\right)\right]$$
$$+B\left[-\frac{1}{2}\left(\frac{x^2-\xi^2}{h^2}\right)Y_0\left(y\frac{1}{(1-s)}\right)+\frac{y(1-s)}{h^2}Y_1\left(y\frac{1}{(1-s)}\right)\right]$$
$$+C\left[-i\frac{\xi x}{h^2}J_0\left(x\frac{1}{(1-s)}\right)+i\frac{\xi(1-s)}{h^2}J_1\left(x\frac{1}{(1-s)}\right)\right]$$
$$+D\left[-i\frac{\xi x}{h^2}Y_0\left(x\frac{1}{(1-s)}\right)+i\frac{\xi(1-s)}{h^2}Y_1\left(x\frac{1}{(1-s)}\right)\right]=0 \tag{A.6}$$

$$-A\left[yJ_1\left(y\frac{s}{(1-s)}\right)\right]-B\left[yY_1\left(y\frac{s}{(1-s)}\right)\right]-C\left[i\xi J_1\left(x\frac{s}{(1-s)}\right)\right]-D\left[i\xi Y_1\left(x\frac{s}{(1-s)}\right)\right]=0, \tag{A.7}$$

$$A\left[i\xi J_0\left(y\frac{s}{(1-s)}\right)\right]+B\left[i\xi Y_0\left(y\frac{s}{(1-s)}\right)\right]+C\left[i\xi Y_0\left(y\frac{s}{(1-s)}\right)\right]+D\left[xY_0\left(x\frac{s}{(1-s)}\right)\right]=0. \tag{A.8}$$

Fixed-Fixed Model

By rearranging Eqs. (A.2.37), (A.2.38), (A.2.39), and (A.2.40) obtained for fixed-fixed model using dimensionless parameters and variables, the following equations are obtained.

$$-A\left[yJ_1\left(y\frac{s}{(1-s)}\right)\right]-B\left[yY_1\left(y\frac{s}{(1-s)}\right)\right]-C\left[i\xi J_1\left(x\frac{s}{(1-s)}\right)\right]-D\left[i\xi Y_1\left(x\frac{s}{(1-s)}\right)\right]=0, \tag{A.9}$$

$$A\left[i\xi J_0\left(y\frac{s}{(1-s)}\right)\right]+B\left[i\xi Y_0\left(y\frac{s}{(1-s)}\right)\right]+C\left[i\xi Y_0\left(y\frac{s}{(1-s)}\right)\right]+D\left[xY_0\left(x\frac{s}{(1-s)}\right)\right]=0 \tag{A.10}$$

$$-A\left[yJ_1\left(y\frac{1}{(1-s)}\right)\right]-B\left[yY_1\left(y\frac{1}{(1-s)}\right)\right]-C\left[i\xi J_1\left(x\frac{1}{(1-s)}\right)\right]-D\left[i\xi Y_1\left(x\frac{1}{(1-s)}\right)\right]=0 \tag{A.11}$$

$$A\left[i\xi J_0\left(y\frac{1}{(1-s)}\right)\right]+B\left[i\xi Y_0\left(y\frac{1}{(1-s)}\right)\right]+C\left[i\xi Y_0\left(y\frac{1}{(1-s)}\right)\right]+D\left[xY_0\left(x\frac{1}{(1-s)}\right)\right]=0. \tag{A.12}$$

Free-Fixed Model

By rearranging Eqs. (A.2.33), (A.2.34), (A.2.39), and (A.2.40) obtained for free-fixed model using dimensionless parameters and variables, the following equations are obtained.

$$\begin{aligned}&A\left[-2i\frac{\xi y}{h^2}J_1\left(y\frac{s}{(1-s)}\right)\right]+B\left[-2i\frac{\xi y}{h^2}Y_1\left(y\frac{s}{(1-s)}\right)\right]\\&+C\left[-\left(x^2-\xi^2\right)\frac{1}{h^2}J_1\left(x\frac{s}{(1-s)}\right)\right]+D\left[-\left(x^2-\xi^2\right)\frac{1}{h^2}Y_1\left(x\frac{s}{(1-s)}\right)\right]=0,\end{aligned} \tag{A.13}$$

$$\begin{aligned}&A\left[-\frac{1}{2}\left(\frac{x^2-\xi^2}{h^2}\right)J_0\left(y\frac{s}{(1-s)}\right)+\frac{y(1-s)}{h^2 s}J_1\left(y\frac{s}{(1-s)}\right)\right]\\&+B\left[-\frac{1}{2}\left(\frac{x^2-\xi^2}{h^2}\right)Y_0\left(y\frac{s}{(1-s)}\right)+\frac{y(1-s)}{h^2 s}Y_1\left(y\frac{s}{(1-s)}\right)\right]\\&+C\left[-i\frac{\xi x}{h^2}J_0\left(x\frac{s}{(1-s)}\right)+i\frac{\xi(1-s)}{h^2 s}J_1\left(x\frac{s}{(1-s)}\right)\right]\\&+D\left[-i\frac{\xi x}{h^2}Y_0\left(x\frac{s}{(1-s)}\right)+i\frac{\xi(1-s)}{h^2 s}Y_1\left(x\frac{s}{(1-s)}\right)\right]=0\end{aligned} \tag{A.14}$$

$$-A\left[yJ_1\left(y\frac{1}{(1-s)}\right)\right]-B\left[yY_1\left(y\frac{1}{(1-s)}\right)\right]-C\left[i\xi J_1\left(x\frac{1}{(1-s)}\right)\right]-D\left[i\xi Y_1\left(x\frac{1}{(1-s)}\right)\right]=0, \tag{A.15}$$

$$A\left[i\xi J_0\left(y\frac{1}{(1-s)}\right)\right]+B\left[i\xi Y_0\left(y\frac{1}{(1-s)}\right)\right]+C\left[i\xi Y_0\left(y\frac{1}{(1-s)}\right)\right]+D\left[xY_0\left(x\frac{1}{(1-s)}\right)\right]=0. \tag{A.16}$$

Shooting Method

Let x_m^r denote the parameters to be optimized, and let $f_m^p\left(x_m^1, x_m^2, \ldots\ldots, x_m^n\right)$ represent the control functions required for the optimization $(r = 1, 2, \ldots, n)$. Here, m denotes the iteration number $(1, 2, \ldots, \infty)$, x_0^i represents the estimated initial value, and f_0^i denotes the known objective function. Let Δx_m^r be the parameter increment ratio. The matrix D, composed of the partial derivatives $\left(\frac{\partial f_m^p}{\partial x_m^r}\right)$ of the function f_m^p with respect to the variable x_m^r, is calculated using Eq. (A.17).

$$\frac{\partial f_m^p}{\partial x_m^r} = \frac{f_{m-1}^p\left(x_{m-1}^1, x_{m-1}^r, \ldots\ldots, x_{m-1}^n\right) - f_m^p\left(x_m^1, x_m^r + \Delta x_m^r, \ldots\ldots, x_m^n\right)}{\Delta x_m^r}. \tag{A.17}$$

The matrix D is therefore written as

$$D = \frac{\partial f_m^p}{\partial x_m^r} = \begin{bmatrix} \frac{\partial f_m^1}{\partial x_m^1} & \frac{\partial f_m^1}{\partial x_m^2} & \frac{\partial f_m^1}{\partial x_m^3} \\ \frac{\partial f_m^2}{\partial x_m^1} & \frac{\partial f_m^2}{\partial x_m^2} & \frac{\partial f_m^2}{\partial x_m^3} \\ \frac{\partial f_m^3}{\partial x_m^1} & \frac{\partial f_m^3}{\partial x_m^2} & \frac{\partial f_m^3}{\partial x_m^3} \end{bmatrix}. \tag{A.18}$$

Let df_m^p denote the difference between the objective function and the function's iteration value. The solution of the linear system of equations given by Eqs. (A.20–A.21) provides the vector δX_m (Eq. A.21), which is defined as the changes to be made in the optimization parameters.

$$\delta X_m = \begin{bmatrix} x_{m+1}^1 - x_m^1 \\ x_{m+1}^2 - x_m^2 \\ x_{m+1}^3 - x_m^3 \end{bmatrix}, \tag{A.19}$$

$$df_m^p = F^p\left(x^1, x^2, \ldots\ldots, x^n\right) - f_m^p\left(x_m^1, x_m^r, \ldots\ldots, x_m^n\right), \tag{A.20}$$

$$\Gamma = df_m^p = \begin{bmatrix} df_m^1 \\ df_m^2 \\ df_m^3 \end{bmatrix}. \tag{A.21}$$

Thus, the linear system can be written as

$$[\mathrm{D}][\delta X] = [\Gamma]. \tag{A.22}$$

Let x_{m+1}^r denote the new iteration value, which is calculated using Eq. (A.23). In multi-parameter systems, changes in the parameters may have unexpected effects. Therefore, a relaxation factor is included when calculating the new iteration value. In Eq. (A.23), s is known as the relaxation factor and takes a value between 0 and 1.

$$[X_{m+1}] = [X_m] + s[\delta X_m], \tag{23}$$

$$x_{m+1}^r = x_m^r + s\delta x_m^r.$$

FUNDING

This work was supported by Scientific Research Projects Coordination Unit of Istanbul University-Cerrahpasa. Project number: FBG-2023-36955.

CONFLICT OF INTEREST

The authors of this work declare that they have no conflicts of interest.

REFERENCES

1. M. Cammalleri and A. Castellano, "A dynamic matrix for the study of free vibrations of thin circular cylindrical shells under different boundary conditions," Designs **7** (6), 122 (2023). https://doi.org/10.3390/designs7060122
2. X. Li, H. Zhang, H. Yang, et al., "Free vibration characteristics of integrated fluted-core composite sandwich cylinders," Compos. Struct. **327**, 117691 (2024). https://doi.org/10.1016/j.compstruct.2023.117691

3. M. J. Jweeg, O. S. Al-Sahib, M. A. Al-Waily, et al., "Free vibration analysis of composite cylindrical shell reinforced with silicon nano-particles: Analytical and FEM approach," Phys. Chem. Solid State. **24** (1), 26–33 (2023). https://doi.org/10.15330/pcss.24.1.26-33
4. P. F. H. Han, Y. Wang, S. F. Chen, et al., "Free vibration of CFRC lattice-core sandwich cylinder with attached mass," Compos. Sci. Technol. **118**, 226–235 (2015). https://doi.org/10.1016/j.compscitech.2015.09.007
5. D. C. Gazis, "Three-dimensional investigation of the propagation of waves in hollow circular cylinders. I. Analytical foundation," J. Acoust. Soc. Am. **31** (5), 568–573 (1959). https://doi.org/10.1121/1.1907753
6. A. E. Armenàkas, D. C. Gazis, and G. Herrmann, *Free Vibrations of Circular Cylindrical Shells* (Elsevier, 2013).
7. H. D. McNiven, A. H. Shah, and J. L. Sackman, "Axially symmetric waves in hollow, elastic rods: Part I," J. Acoust. Soc. Am. **40** (4), 784–792 (1966). https://doi.org/10.1121/1.1910190
8. J. R. Hutchinson, "Vibrations of solid cylinders," J. Appl. Mech. **47**, 901–907 (1980). https://doi.org/10.1115/1.3153811
9. S. Guo and S. Yang, "Free longitudinal vibrations of non-uniform rods," Sci. China Technol. Sci. **54**, 2735–2745 (2011). https://doi.org/10.1007/s11431-011-4534-6
10. A. K. Ghosh, "Axisymmetric vibration of a long cylinder," J. Sound Vib. **186** (5), 711–721 (1995). https://doi.org/10.1006/jsvi.1995.0484
11. M. Eisenberger, "Exact longitudinal vibration frequencies of a variable cross-section rod," Appl. Acoust. **34** (2), 123–130 (1991). https://doi.org/10.1016/0003-682X(91)90027-C
12. S. Abrate, "Vibration of non-uniform rods and beams," J. Sound Vib. **185** (4), 703–716 (1995). https://doi.org/10.1006/jsvi.1995.0410
13. B. Kumar and R. Sujith, "Exact solutions for the longitudinal vibration of non-uniform rods," J. Sound Vib. **207** (5), 721–729 (1997). https://doi.org/10.1006/jsvi.1997.1146
14. A. Raj and R. Sujith, "Closed-form solutions for the free longitudinal vibration of inhomogeneous rods," J. Sound Vib. **283** (3), 1015–1030 (2005). https://doi.org/10.1016/j.jsv.2004.06.003
15. G. Gladwell and D. Vijay, "Natural frequencies of free finite-length circular cylinders," J. Sound Vib. **42** (3), 387–397 (1975). https://doi.org/10.1016/0022-460X(75)90252-7
16. A. Farshidianfar and P. Oliazadeh, "Free vibration analysis of circular cylindrical shells: Comparison of different shell theories," Int. J. Mech. Appl. **2** (5), 74–80 (2012). https://doi.org/10.5923/j.mechanics.20120205.04
17. M. Asgari, "Free vibration analysis of functionally heterogeneous hollow cylinder based on three-dimensional elasticity theory," Int. J. Acoust. Vib. **22** (2), 151–160 (2017). https://doi.org/10.20855/ijav.2017.22.2460
18. X.-Y. Miao, Y.-L. Li, C.-F. Jiang, and Z.-X. Zhang, "Free vibration analysis of three-layer thin cylindrical shell with variable thickness two-dimensional FGM middle layer under arbitrary boundary conditions," J. Sandwich Struct. Mater. **24** (2), 973–1003 (2022). https://doi.org/10.1177/10996362211020429
19. V. N. Paimushin and V. M. Shishkin, "Refined model of dynamic deformation of a flat rod with a finite-length fixed region on an outer surface," J. Appl. Mech. Tech. Phys. **65** (1), 161–175 (2024). https://doi.org/10.1134/S0021894424010176
20. G. S. Leizerovich and N. A. Taranukha, "Nonobvious features of dynamics of circular cylindrical shells," Mech. Solids **43** (2), 246–253 (2008). https://doi.org/10.3103/S0025654408020106
21. A. M. Akhtyamov, A. V. Muftakhov, M. Taikher, and L. S. Yamilova, "On a method for determining the fixing conditions for a rectangular plate from the natural frequencies," Mech. Solids **42** (1), 85–96 (2007). https://doi.org/10.3103/S0025654407010116
22. J. R. Hutchinson and S. A. El-Azhari, "Vibrations of free hollow circular cylinders," J. Appl. Mech. **53** (3), 641–646 (1986). https://doi.org/10.1115/1.3171824
23. A. Houmat and J. Hutchinson, "Free vibration of bodies of revolution by boundary collocation," J. Sound Vib. **171** (1), 35–48 (1994). https://doi.org/10.1006/jsvi.1994.1102

24. D. D. Ebenezer, K. Ravichandran, and C. Padmanabhan, "Free and forced vibrations of hollow elastic cylinders of finite length," J. Acoust. Soc. Am. **137** (5), 2927–2938 (2015). https://doi.org/10.1121/1.4919339
25. J. N. Sharma and Y. D. Sharma, "Free vibration analysis of an eccentric thermoelastic hollow cylinder," J. Therm. Stress. **35** (11), 976–999 (2012). https://doi.org/10.1080/01495739.2012.720217
26. T. V. Grishanina and F. N. Shklyarchuk, "Use of the Riesz method to calculate axisymmetric vibrations of composite shells of revolution supported by rings and filled with a liquid," Mech. Solids **51** (3), 357–369 (2016). https://doi.org/10.3103/S0025654416030134
27. C. Wang and J. Lai, "Prediction of natural frequencies of finite length circular cylindrical shells," Appl. Acoust. **59** (4), 385–400 (2000). https://doi.org/10.1016/S0003-682X(99)00039-0
28. R. Singh, A. Gupta, and N. K. Jain, "Free vibration analysis of cracked isotropic and FGM cylindrical shells with axially varying thickness: An analytical approach," Thin-Walled Struct. **214**, 113344 (2025). https://doi.org/10.1016/j.tws.2024.113344
29. A. Rawat, V. A. Matsagar, and A. K. Nagpal, "Free vibration analysis of thin circular cylindrical shell with closure using finite element method," Int. J. Steel Struct. **20** (1), 175–193 (2020). https://doi.org/10.1007/s13296-019-00277-5
30. C.-P. Wu and S.-W. Yang, "A semi-analytical element-free Galerkin method for the 3D free vibration analysis of multilayered FGM circular hollow cylinders," J. Intell. Mater. Syst. Struct. **22** (17), 1993–2007 (2011). https://doi.org/10.1177/1045389X11421822
31. S. M. R. Khalili, A. Davar, and K. Malekzadeh Fard, "Free vibration analysis of homogeneous isotropic circular cylindrical shells based on a new three-dimensional refined higher-order theory," Int. J. Mech. Sci. **56** (1), 1–25 (2012). https://doi.org/10.1016/j.ijmecsci.2011.11.002
32. M. Mofakhami, H. H. Toudeshky, and S. H. Hashemi, "Finite cylinder vibrations with different end boundary conditions," J. Sound Vib. **297** (1), 293–314 (2006). https://doi.org/10.1016/j.jsv.2006.03.041
33. V. Yıldırım, "Kalın cidarlı içi boş silindirlerin doğal frekanslarınınn dış/iç çap oranı ve sınır şartları ile değişimi," GİDB Dergi. **15**, 3–12 (2019).
34. S. M. Hasheminejad and A. Ghaheri, "Free vibration analysis of a finite-length isotropic solid elliptic cylinder using exact three dimensional elasticity theory," Appl. Math. Model. **37** (20), 8725–8741 (2013). https://doi.org/10.1016/j.apm.2013.03.066
35. D. Sharma and H. Mittal, "Analysis of free vibrations of axisymmetric functionally graded generalized viscothermoelastic cylinder using series solution," J. Vib. Eng. Technol. **8**, 783–798 (2020). https://doi.org/10.1007/s42417-019-00178-1
36. O. Aydın and C. Aygün, "On the hydrodynamical development length for pressure-driven pulsating laminar flow in a pipe," Isı Bilimi ve Tekniği Dergisi **34** (1), 3–12 (2014).
37. C. Aygün and O. Aydın, "Pressure-driven laminar pulsating flow in a pipe: Effect of the amplitude," Isı Bilimi ve Tekniği Dergisi **35** (1), 97–105 (2015).
38. E. Ceryan and M. Yürüsoy, "Boru içerisindeki bir akış problemine ait analitik ve nümerik çözümler," Afyon Kocatepe Üniversitesi Fen Mühendislik Bilimleri Dergisi **12** (1), 1–9 (2012).
39. S. R. Atashipour, Z. Mohammadi, and P. D. Folkow, "A direct approach for three-dimensional elasto-static and elasto-dynamic solutions in curvilinear cylindrical coordinates with application to classical cylinder problems," Eur. J. Mech.–A/Solids **95**, 104646 (2022). https://doi.org/10.1016/j.euromechsol.2022.104646
40. I. Keles and N. Tutuncu, "Exact analysis of axisymmetric dynamic response of functionally graded cylinders (or disks) and spheres," J. Appl. Mech. **78** (6), 061014 (2011). https://doi.org/10.1115/1.4003914
41. V. N. Paimushin and V. M. Shishkin, "Deformation of thin-walled structural elements having fixed areas of finite dimensions on the boundary front surfaces," J. Appl. Mech. Tech. Phys. **64** (2), 308–324 (2023). https://doi.org/10.1134/S0021894423020153
42. G. M. Sevastyanov, O. N. Komarov, and A. V. Popov, "Torsion and circular shear coupling in a nonlinear elastic hollow cylinder," Mech. Solids **60** (1), 136–145 (2025). https://doi.org/10.1134/S0025654424605366
43. A. L. Popov, A. O. Vatulyan, D. A.Chelyubeyev, et al.,"On the solution of the problem of axial compression of an elastic cylinder with specified end displacement conditions,"Mech. Solids **60**, 912–922 (2025). https://doi.org/10.1134/S0025654424605937
44. V. Sharma, D.K. Sharma, N.Sarkar, et al.,"Investigation on transient viscothermoelastic waves in a half-space due to instantaneous thermal point heat sources via Moore–Gibson–Thompson heat conduction," Mech. Sol-

ids **60**, 2841–2857 (2025).
https://doi.org/10.1134/S0025654425600758

45. J. He, "Transient response of a hollow cylinder with nonlocal effect and fractional thermoelasticity," Mech. Solids **60**, 1117–1129 (2025).
https://doi.org/10.1134/S002565442560028X
46. G. A. Yahya, F. S. Bayones, and A. M. Abd-Alla, "Analytical investigation of harmonic magnetoelastic stress distribution in a functionally graded infinite cylinder," Mech. Solids **60**, 4673–4686 (2025).
https://doi.org/10.1134/S0025654425601934
47. P. Yu, D. Yang, L.Peng, et al.,"Analysis of flexoelectric hollow cylinder with thermopolarization effect," Mech. Solids **59**, 3024–3037 (2024).
https://doi.org/10.1134/S0025654424605068
48. D. D. Morrison, J. D. Riley, and J. F. Zancanaro, "Multiple shooting method for two-point boundary value problems," Commun. ACM **5** (12), 613–614 (1962).
https://doi.org/10.1145/355580.369128
49. M. R. Osborne, "On shooting methods for boundary value problems," J. Math. Anal. Appl. **27** (2), 417–433 (1969).
https://doi.org/10.1016/0022-247X(69)90059-6
50. Q. M. Al-Mdallal, M. I. Syam, and M. N. Anwar, "A collocation-shooting method for solving fractional boundary value problems," Commun. Nonlinear Sci. Numer. Simul. **15** (12), 3814–3822 (2010).
https://doi.org/10.1016/j.cnsns.2010.01.020
51. S. N. Ha, "A nonlinear shooting method for two-point boundary value problems," Comput. Math. Appl. **42** (10–11), 1411–1420 (2001).
https://doi.org/10.1016/S0898-1221(01)00250-4
52. L. Fang, S. Vandewalle, and J. Meyers, "An SQP-based multiple shooting algorithm for large-scale PDE-constrained optimal control problems," J. Comput. Phys. **477**, 111927 (2023).
https://doi.org/10.1016/j.jcp.2023.111927

Publisher's Note. Pleiades Publishing remains neutral with regard to jurisdictional claims in published maps and institutional affiliations.
AI tools may have been used in the translation or editing of this article.